IEEE Photonics Journal
An IEEE Photonics Society Publication

Study on a DFB Laser Diode Based on Sampled Grating Technique for Suppression of the Zeroth Order Resonance

Volume 9, Number 2, April 2017

Lianyan Li
Yuechun Shi
Yunshan Zhang
Hui Zou
Jianping Shen
Xiangfei Chen

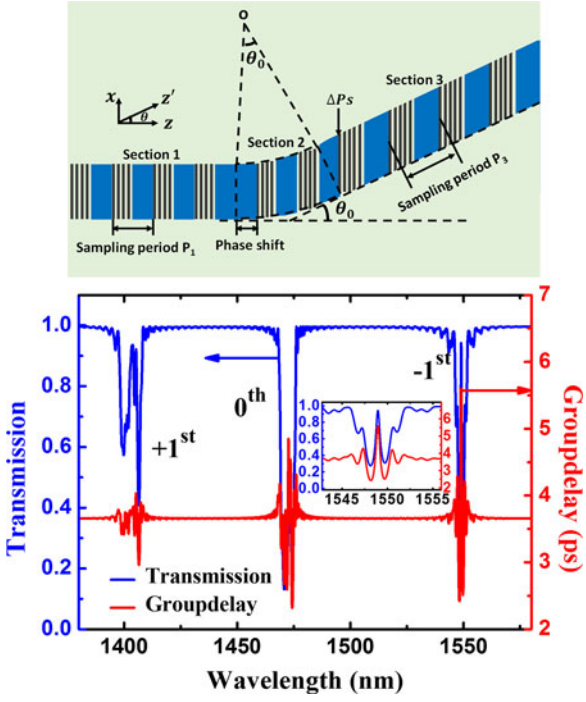

DOI: 10.1109/JPHOT.2017.2686430
1943-0655 © 2017 IEEE

Study on a DFB Laser Diode Based on Sampled Grating Technique for Suppression of the Zeroth Order Resonance

Lianyan Li,[1,2] Yuechun Shi,[2] Yunshan Zhang,[1,2] Hui Zou,[1] Jianping Shen,[1] and Xiangfei Chen[2]

[1]School of Optoelectronic Engineering, Nanjing University of Posts and Telecommunications, Nanjing 210023, China
[2]College of Engineering and Applied Sciences, Nanjing University, Nanjing 210009, China

DOI:10.1109/JPHOT.2017.2686430

Manuscript received February 16, 2017; revised March 15, 2017; accepted March 19, 2017. Date of publication March 28, 2017; date of current version April 7, 2017. This work was supported in part by the Nature Science Foundation of Jiangsu Province of China under Grant BK20160907, Grant BK20140414, and Grant BK20141168; in part by the National "863" project of China (2015AA016902); in part by the National Natural Science Foundation of China under Grant 61435014, Grant 61504058, Grant 61504170, and Grant 61640419; and in part by Nanjing University of Posts and Telecommunications Foundation under Grant NY216013, Grant NY215007, and Grant NY215113.) Corresponding author: Y. Shi (e-mail: shiyc@nju.edu.cn).

Abstract: A distributed feedback (DFB) semiconductor laser based on sampled grating with multiple sections, i.e., a straight, a bent, and a tilted waveguide, is proposed to suppress the 0th-order resonance. A sampling structure with nonlinear equivalent chirp pattern is carefully designed to compensate the basic grating chirp introduced by the bent and tilted waveguide. The facet reflection can also be reduced due to the tilted waveguide to avoid the influence of random facet phase. As a result, good single longitudinal mode (SLM) property and high wavelength accuracy in the −1st-order subgrating is achieved, even with a large sampling period. Because the lasing wavelength can be easily adjusted by a sampling period and the fabrication accuracy requirement is relaxed, it will benefit the realization of low-cost DFB laser arrays with a good SLM property and accurate lasing wavelength.

Index Terms: Distributed feedback (DFB) semiconductor laser, sampled grating technique, bent waveguide.

1. Introduction

Multiwavelength distributed feedback (DFB) semiconductor laser is a key element in wavelength division multiplexing (WDM) systems and large-scale photonics integrated circuits (PICs) [1]. The traditional method to fabricate a laser array is using electron beam lithography (EBL) which can write arbitrary grating patterns point by point. However, it is still challenging to control the wavelength deviation with very high accuracy. For instance, if the wavelength deviation within ±0.2 nm is required, the grating pitch difference should be as small as around 0.03 nm, which is a tough task for EBL. In addition, EBL also suffers from time consuming and high cost, which limits its volume fabrication to some extent [2]. In order to overcome these problems, some other methods such as bent waveguide [3], varied waveguide width [4], asymmetric sampled grating [5] and nanoimprint [6]

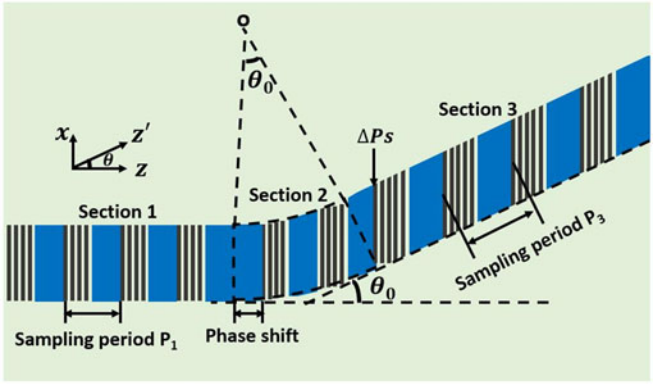

Fig. 1. Schematic of the proposed laser structure with a straight waveguide, a bent waveguide, and a tilted waveguide.

have been proposed. Among them, bent waveguide and varied waveguide width have the advantage of easy fabrication, but the varied wavelength range is limited to a few nanometers. The asymmetric sampled grating is an efficient way to achieve large wavelength range, but it is hard to realize the index shifter accurately. In order to simultaneously realize easy fabrication, high wavelength accuracy and wide wavelength range, a sampled grating technique which is called reconstruction equivalent chirp (REC) technique was proposed [7]. Based on REC technique, DFB laser arrays with high performance have been experimentally demonstrated [8,9]. The recently reported wavelength deviation can be controlled within as small as $\pm$0.1 nm [10]. However, according to Fourier analysis, multi-channel response (or multiple subgratings) takes place in such a structure. In order to ensure single longitudinal mode (SLM) operation, the sampling period should be small enough to make the 0th order wavelength far away from the gain region, and only leaving the $+$1st or $-$1st order wavelength in the gain region for light resonance. This feature sometimes limits its applications. For example, when the required lasing wavelength is small or the gain bandwidth is relatively large, the sampling period has to be small enough, which still increases the fabrication cost and reduces the design flexibility. Therefore, the suppression of 0th order resonance remains an important task. Some methods have been proposed to suppress the 0th order resonance, such as periodic injection blocking [11], anti-symmetric-sample structure [12], multiexposure technique [13] and asymmetrical sampling structure [14]. However, the fabrication of those structures are all complicated, for example, accurate material growth must be ensured in the injection blocking layer and precise mask alignment should be applied in the grating fabrication of multiexposure technique.

In this paper, we propose a new multi-section structure with a straight, a bent and a tilted waveguide to suppress the 0th order resonance. A nonlinear equivalently chirped sampling pattern is designed, which is the first time to our knowledge, to compensate the grating chirp introduced by the bent and tilted waveguide, resulting in a uniform $-$1st order subgrating period. An π equivalent phase shift (π-EPS) is also inserted to ensure SLM property. Due to the large size property of the sampling structure and waveguide structure, it can be easily fabricated by holographic exposure and conventional photolithography. The proposed waveguide structure can be fabricated by the processes of common straight waveguide structures. Therefore, the proposed method has advantages of easy fabrication and low cost [15].

2. Principle

The proposed laser is divided into three sections as shown in Fig. 1. All of them share the same uniform basic grating with period Λ_0 along z direction. Section 1 is a straight waveguide with sampling period P_1. Section 2 is a bent waveguide with a tilt angle varying from 0 to θ_0. Section 3 is a tilted waveguide with a tilt angle θ_0 and sampling period P_3, which is along the direction of z'.

Therefore, the effective grating period in Section 3 along z' can be expressed as

$$\Lambda\left(z'\right)=\frac{\Lambda_0}{\cos\theta_0}. \tag{1}$$

It can be seen that the period of the 0th order subgrating in Section 3 is a little longer than that in Sections 2 and 1, which makes the 0th order resonances of different sections deviated. And hence it can be suppressed. Here, the -1st order subgrating is used for light resonance. Therefore, the sampling periods in these three sections should be carefully designed to make the -1st order subgrating equivalently uniform. In addition, π-EPS and the tilt angle should also be carefully designed to obtain good SLM operation.

According to Fourier analysis, the index modulation of the sampled grating in Section 1 can be expressed as [16]

$$\Delta n\left(z\right)=\frac{1}{2}\Delta n_s\sum_m F_m\exp\left[j2\pi\left(\frac{1}{\Lambda_0}+\frac{m}{P_1}\right)z\right]+c.c \tag{2}$$

where Δn_s is the index modulation of the basic grating, m denotes the order of Fourier series, and F_m is the Fourier coefficient of the m^{th} order subgrating.

When the -1st order subgrating is used as working grating, the effective grating period Λ_{-1} can be calculated as

$$\frac{1}{\Lambda_{-1}}=\frac{1}{\Lambda_0}-\frac{1}{P_1}. \tag{3}$$

Then, combining (1), the relationship in Section 3 can be simply expressed as

$$\frac{1}{\Lambda_{-1}}=\frac{\cos\theta_0}{\Lambda_0}-\frac{1}{P_3}. \tag{4}$$

In order to link Sections 1 and 3 and lower the radiation loss, arc-shaped Section 2 is used here. Because of the arc-shape, the effective grating period changes along the waveguide. As a result, nonlinear grating chirp is introduced in the -1st order subgrating. Here, a nonlinear chirped sampling pattern is designed to compensate the basic grating chirp. The effective grating period in this section can be expressed as

$$\Lambda\left(z\right)=\frac{\Lambda_0}{\sqrt{1-\left(\frac{z}{R}\right)^2}}. \tag{5}$$

where R is the radius of curvature (ROC) of the bent waveguide. The grating index modulation can be expressed as

$$\Delta n\left(z\right)=\frac{1}{2}\Delta n_s\exp\left[j2\pi\left(\int_0^z\frac{1}{\Lambda\left(z'\right)}dz'\right)\right]+c.c\approx\frac{1}{2}\Delta n_s\exp\left(j2\pi\frac{z}{\Lambda_0}\right)\exp\left(-j2\pi\frac{1}{6\Lambda_0R^2}z^3\right)+c.c. \tag{6}$$

Generally, the sampling pattern with arbitrary phase change can be expanded as

$$S\left(z\right)=\sum_m F_m\exp\left[j\frac{2\pi m}{P_1}\left(z+\varphi\left(z\right)\right)\right] \tag{7}$$

where $\varphi(z)$ is phase shift of the m^{th} order subgrating. When $\varphi(z)=0$, (7) is reduced to be a uniform sampled grating. For the -1st order subgrating, the index modulation is expressed as

$$\Delta n_{-1}\left(z\right)=\frac{1}{2}\Delta n_sF_{-1}\exp\left[j2\pi\left(\frac{1}{\Lambda_0}-\frac{1}{P_1}\right)z\right]\exp\left[-j\pi\left(\frac{1}{3\Lambda_0R^2}z^3+\frac{2}{P_1}\varphi\left(z\right)\right)\right]+c.c. \tag{8}$$

From (6) and (8), if a specifically designed sampling pattern is used to compensate the grating chirp in the -1st order subgrating, the following condition must be satisfied:

$$\frac{1}{3\Lambda_0 R^2} z^3 + \frac{2}{P_1}\varphi(z) = 0. \tag{9}$$

Therefore, we can get the phase function $\varphi(z)$ in sampling structure as

$$\varphi(z) = -\frac{z^3 P_1}{6\Lambda_0 R^2}. \tag{10}$$

Now the start position of each sampling period can be obtained from

$$z - \frac{z^3 P_1}{6\Lambda_0 R^2} = N P_1 \tag{11}$$

where N is an integer, which means the N^{th} sampling period.

Then, we can get an equivalently uniform grating with index modulation as

$$\Delta n_{-1}(z) = \frac{1}{2}\Delta n_s F_{-1} \exp\left[j2\pi\left(\frac{1}{\Lambda_0} - \frac{1}{P_1}\right)z\right] + c.c. \tag{12}$$

It has the same Bragg wavelength as that in the other sections.

Under such a sampling pattern, the index modulations of the $+1^{st}$ and 0th order subgratings can be expressed as

$$\Delta n_{+1}(z) = \frac{1}{2}\Delta n_s F_{+1} \exp\left[j2\pi\left(\frac{1}{\Lambda_0} + \frac{1}{P_1}\right)z\right] \exp\left(-j\pi\frac{2}{3\Lambda_0 R^2} z^3\right) + c.c \tag{13}$$

$$\Delta n_0(z) = \frac{1}{2}\Delta n_s F_0 \exp\left[j2\pi\frac{z}{\Lambda_0}\right] \exp\left[-j\pi\frac{1}{3\Lambda_0 R^2} z^3\right] + c.c. \tag{14}$$

It implies that the chirp in the $+1$st order subgrating is doubled, while that in the 0th order subgrating is the same as the basic grating.

The phase of the sampling structure (hereinafter referred to as the sampling phase) at the two interfaces between sections should be carefully designed. In our analysis, the initial sampling phase of Section 1 is assumed to be 0, and the sampling phase change along Section 1 is $2q\pi$, where q is an integer. Then, we introduce a π-EPS between Sections 1 and 2. Since the length of Section 2 is determined by the tilt angle θ_0 and ROC, the sampling phase change along Section 2 is usually not an integral multiple of 2π. Therefore, we should introduce a sampling phase shift term $\exp(-j2m\pi\frac{\Delta P_s}{P_1})$ between Sections 2 and 3 to keep the sampling phase continuous, where $z = Rsin(\theta_0)$.

Therefore, the index modulation of the -1st order subgrating in Section 3 is,

$$\Delta n_{-1}(z) = \frac{1}{2}\Delta n_s F_{-1} \exp\left[j2\pi\left(\frac{\cos\theta_0}{\Lambda_0} - \frac{1}{P_3}\right)z + j2\pi\frac{\Delta P_s}{P_1}\right] + c.c. \tag{15}$$

Then, we can calculate the sampling phase shift ΔP_s by

$$\left(\frac{1}{\Lambda_0} - \frac{1}{P_1}\right)z = \left(\frac{\cos\theta_0}{\Lambda_0} - \frac{1}{P_3}\right)z + \frac{\Delta P_s}{P_1}. \tag{16}$$

From (16) we can get

$$\Delta P_s = \frac{\cos\theta_0}{\Lambda_0} - \frac{1}{P_3} - \frac{1}{\Lambda_0} + \frac{1}{P_1} Y P_1 R \sin\theta_0. \tag{17}$$

3. Design and Simulation

3.1 Waveguide Structure Design

The laser is designed with InP material system. The Epi-wafer structure is shown in Fig. 2(a), where the active material consists of five AlGaInAs quantum wells with $+1.2\%$ tensile strain and

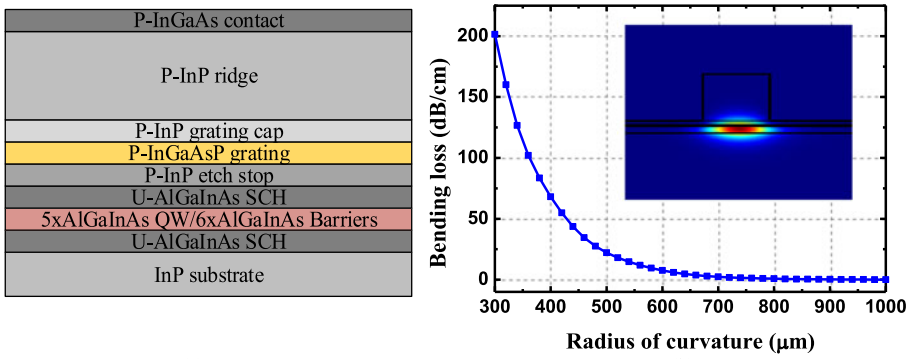

Fig. 2. (a) Material stack of the Epi-wafer. (b) Bending loss of the bent waveguide versus ROC. (inset) Mode profile of the waveguide when the tilt angle is 4°.

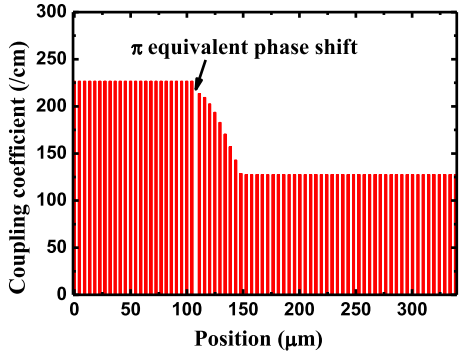

Fig. 3. Coupling coefficient along cavity.

six AlGaInAs barriers with 0.45% compressive strain. The grating layer is InGaAsP quaternary with thickness of 50 nm and photoluminescence wavelength at 1.36 μm. The waveguide width is 1.8 μm.

Since Section 2 is a bent waveguide, the bending losses with different ROC are calculated using MODE solution software [17]. It is shown in Fig. 2(b) that the bending loss increases dramatically with the decrease of ROC. In our waveguide design, the ROC of 600 μm is used, where the radiation loss is 7.58 dB/cm, which means a loss of 0.03 dB is introduced when the tilt angled is 4° ($\theta_0 = 4°$). In addition, the interface between the straight and bent waveguide can also cause loss due to mode mismatch, where the overlap is calculated as 0.96 and the corresponding loss is 0.17 dB. Consequently, the total loss introduced by the bent waveguide is 0.37 dB, including the radiation loss in the bent waveguide region and the scattering loss between sections.

Another important issue in bent waveguide is the varied coupling coefficient which is calculated by [18]

$$\kappa = \frac{\omega\varepsilon_0}{4} \iint \frac{1}{\pi\left(n_1^2 - n_0^2\right) \exp\left(j\frac{2\pi}{\Lambda_0}\cos\theta x\right) U^2(x, y)\, dxdy} \tag{18}$$

where ω is the angular frequency, ε_0 is the dielectric constant in vacuum, n_1 and n_0 are the effective refractive indexes of the grating layer and the cladding layer, and $U(x, y)$ is the mode field distribution. The coupling coefficient of the grating along laser cavity is plotted in Fig. 3. It is 227.1/cm in Section 1 and 127.7/cm in Section 3, whereas in Section 2, the coupling coefficient decreases with the tilt angle. Here, a π-EPS is inserted between Sections 1 and 2. The cavity length is designed to be asymmetric in order to keep the normalized coupling coefficient κL in Section 1

TABLE 1
Parameters Used in the Simulation

Parameters	Values
Cavity length Section 1	108 μm
Cavity length Section 3	192 μm
Seed grating period	228.6 nm
Sampling period 1	4.53 μm
Sampling period 3	4.77 μm
Effective refractive index	3.22
Group index	3.6
Gain constant	1.5×10^5 m^{-1}
Confinement factor	0.08
Linewidth enhancement factor	2.5
Linear carrier lifetime	4 ns
Waveguide loss	15 cm^{-1}
Transparent carrier density	1.0×10^{24} m^{-3}

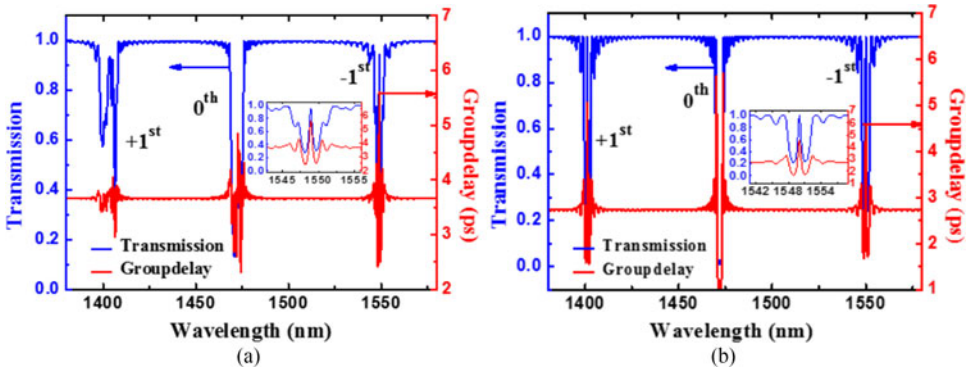

Fig. 4. Transmission spectra and group delays of (a) the proposed multi-section laser. (b) Normal DFB laser with π-EPS. (Insets) Detailed spectra around the -1st order Bragg wavelength.

equals to that in Section 3, in which case the laser has the largest threshold modal gain margin. The other parameters used in the simulation are listed in Table 1.

3.2 Simulation of the Laser Performances

The transmission spectrum and group delay of the waveguide grating is simulated using the Transfer Matrix Method (TMM) [19], where the bending loss and varied coupling coefficient are considered. A nonlinear equivalent chirped sampling pattern is used in Section 2 and a π-EPS is also inserted between Sections 1 and 2. Another sampling phase shift ΔP_s is also inserted between Sections 2 and 3 to achieve a continuous phase change in the -1st order subgrating.

It is shown in Fig. 4(a) that the 0th transmissions of the sections have mismatch due to the tilt angle, so that the bandwidth of the 0th order subgrating is broadened and the group delay of the 0th order resonance (4.849 ps) is lower than that of the -1st order resonance (5.6 ps), which means the

TABLE 2
Threshold and Threshold Modal Gain of the Laser

	Wavelength (nm)	Threshold (mA)	Threshold modal gain (cm^{-1})	Normalized threshold modal gain
−1st Main mode	1550.04	20.6	52.72	1.79
−1st Side mode	1548.40	30.8	84.14	2.86
0th Main mode	1474.36	23.6	63.73	2.17

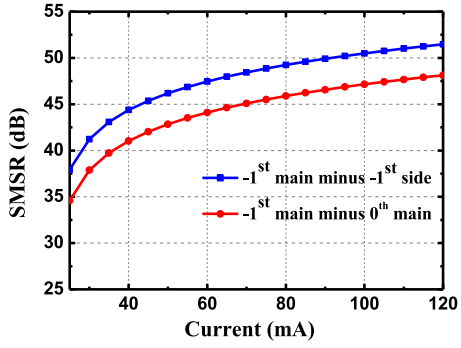

Fig. 5. SMSRs under different currents.

0th order resonance is suppressed to some extent. There is nearly no distortion in the −1st order resonance due to the equivalent chirp compensation and the transmission peak is at the center of the stopband due to the π-EPS. Since the grating chirp in the +1st and 0th order subgratings are not compensated, those two stopbands are distorted. The transmission spectrum and group delay of a normal DFB laser with π-EPS are also simulated and plotted in Fig. 4(b) for comparison. It shows strong resonance in the 0th order subgrating. However, such a strong resonance is missing in the proposed structure as shown in Fig. 4(a), which indicates that the 0th order resonance is well suppressed.

The tilt angle θ_0 is an important parameter of the proposed laser structure. On one hand, it should be large enough to separate the 0th resonances. On the other hand, it should be as small as possible to reduce the radiation loss. So there is a tradeoff. According to the calculation results of group delay, $\theta_0 = 4^\circ$ is selected here. The calculated threshold current and threshold modal gain of the proposed laser are listed in Table 2. The values of the 0th potential lasing mode are also given in Table 2. In addition, the side mode suppression ratios (SMSRs) under different currents are calculated according to [20] and plotted in Fig. 5. The blue line shows the SMSRs between the main mode and side mode for the −1st order subgrating (−1st main minus −1st side) which reaches as high as 50 dB at 90 mA. The red line shows the SMSRs between the main mode in the −1st order subgrating and main mode in the 0th order subgrating (−1st main minus 0th main), which is about 3 dB lower than the former curve. Noted that the material gain is assumed to be the same in the 0th and −1st order wavelength in the calculation. In the practical situation, the material gain in the 0th order wavelength is usually much smaller than that in the −1st order wavelength, therefore the SMSR between −1st and 0th order subgrating should be much larger.

The L-I curve of the laser and photon distributions are also simulated using the TMM method [19]. It is shown in Fig. 6(a) that the threshold current is around 20.6 mA, and the slop efficiencies of the front and rear facets are 0.30 W/A and 0.35 W/A respectively. Because the laser cavity is

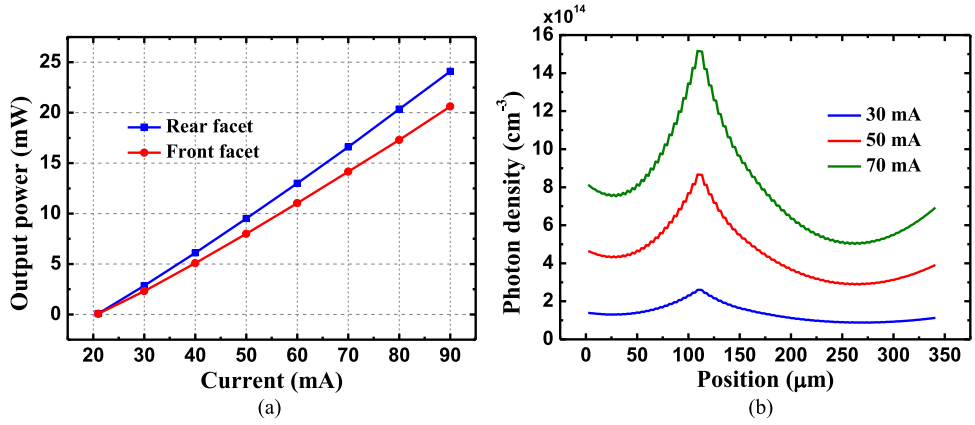

Fig. 6. (a) L-I curves from the rear and front laser facets. (b) Photon distributions in the cavity.

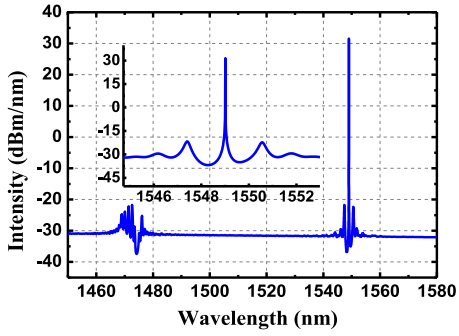

Fig. 7. Spectrum of the proposed laser structure. (Inset) Lasing spectrum around the −1st stopband.

asymmetric and the π-EPS is more close to the rear facet (36% of the cavity length), there are more light extracted from the rear facet. The photon density distributions at different injection currents are plotted in Fig. 6(b). It is clear to see that more light is accumulated at the phase shift position, which is in accordance with Fig. 6(a). It should be noted that the longitudinal spatial hole burning (SHB) is an intrinsic problem for all lasers with phase shift gratings, and it can be reduced by designing the grating structures in the proposed laser such as equivalent corrugation pitch modulated (CPM), equivalent multiple phase shifts (MPS), and so on.

Fig. 7 is the calculated spectrum of the proposed laser at an injection current of 40 mA. It can be seen that the 0th resonance is well suppressed. The inserted figure shows the detailed curve of the −1st order lasing spectrum. The lasing wavelength is in the middle of the stopband, showing the grating chirp is well compensated.

4. Discussions

In the practical applications, the −1st lasing wavelength is designed at the peak wavelength of the gain material, and the 0th wavelength is designed to be more than 50 nm away from the lasing wavelength. Therefore, the material gain of the 0th order wavelength is actually much smaller than that of the −1st order wavelength. Therefore, better effect of the 0th order suppression can be expected.

The lasing wavelength accuracy is one of the key features for the laser arrays. In the sampled grating technique, wavelength can be controlled by the sampling period. Hence, the multiwavelength DFB laser array can be easily achieved. In addition, the facet reflection can seriously influence the

lasing wavelength [21]. Usually, antireflection coatings must be applied to avoid the random facet phase. However, to further reduce the facet reflection, tiled waveguide is a good method [11]. Thanks to the tilted waveguide in the proposed structure, the facet reflectivity can be reduced to achieve good wavelength accuracy. Besides, more light can be extracted in one facet due to the grating asymmetry, leading to a better light efficiency.

5. Conclusion

A multi-section DFB laser structure is proposed to suppress the 0th order resonance of the sampled grating to improve the SLM property and relax the fabrication accuracy requirement. A nonlinear equivalent chirp is designed to compensate the basic grating chirp in the bent waveguide. The simulation results show that the proposed laser has good SLM property. Since the sampled grating and the proposed waveguide structure can be fabricated by holographic exposure and conventional photolithography, the laser can be easily fabricated by common processes. Therefore, it is beneficial for the multiwavelength laser array in DWDM systems and PICs.

References

[1] R. Nagarajan *et al.*, "Large-scale photonic integrated circuits," *IEEE J. Sel. Topics Quantum Electron.*, vol. 11, no. 1, pp. 50–65, Jan./Feb. 2005.

[2] T. Lee *et al.*, "Multiwavelength DFB laser array transmitters for ONTC reconfigurable optical network testbed," *J. Lightw. Technol.*, vol. 14, no. 6, pp. 967–976, Jun. 1996.

[3] H. Hillmer and B. Klepser, "Low-cost edge-emitting DFB laser arrays for DWDM communication systems implemented by bent and tilted waveguides," *IEEE J. Quantum Electron.*, vol. 40, no. 10, pp. 1377–1383, Oct. 2004.

[4] G. P. Li, T. Makino, and C. M. Wu, "Multi-ridge waveguide gain-coupled DFB laser array," *J. Lightw. Technol.*, vol. 13, no. 2, pp. 196–199, Feb. 1995.

[5] S.-W. Ryu, S.-B. Kim, J.-S. Sim, and J. Kim, "Monolithic integration of a multiwave length laser array associated with asymmetric sampled grating lasers," *IEEE J. Sel. Topic Quantum Electron.*, vol. 8, no. 6, pp. 1358–1365, Nov./Dec. 2002.

[6] J. Zhao *et al.*, "Experimental demonstration of a 16-channel DFB laser array based on nanoimprint technology," *Semicond. Sci. Technol.*, vol. 28, no. 5, May 2013, Art. no. 055015.

[7] Y. Dai and X. Chen, "DFB semiconductor lasers based on reconstruction-equivalent-chirp technology," *Opt. Exp.*, vol. 15, no. 5, pp. 2348–2353, Mar. 2007.

[8] Y. Shi *et al.*, "High channel count and high precision channel spacing multi-wavelength laser array for future PICs," *Sci. Rep.*, vol. 4, Dec. 2014, Art. no. 7377.

[9] Y. Shi *et al.*, "Experimental demonstration of eight-wavelength distributed feedback semiconductor laser array using equivalent phase shift," *Opt. Lett.*, vol. 37, no. 16, pp. 3315–3317, Aug. 2012.

[10] J. Lu *et al.*, "Multi-wavelength distributed feedback laser array with very high wavelength-spacing precision," *Opt. Lett.*, vol. 40, no. 22, pp. 5136–5139, Nov. 2015.

[11] S. Bao, Y. Xi, S. Zhao, and X. Li, "Sampled grating DFB laser array by periodic injection blocking," *IEEE J. Sel. Topics Quantum Electron.*, vol. 19, no. 5, Sep./Oct. 2013, Art. no. 1503008.

[12] Y. Shi *et al.*, "An anti-symmetric-sample grating structure for improving the reconstruction-equivalent-chirp technology," *IEEE Photon. Technol. Lett.*, vol. 23, no. 18, pp. 1337–1339, Sep. 2011.

[13] J. Li *et al.*, "A multiexposure technology for sampled Bragg gratings and its applications in dual-wavelength lasing generation and OCDMA en/decoding," *IEEE Photon. Technol. Lett.*, vol. 21, no. 21, pp. 1639–1641, Nov. 2009.

[14] Y. Zhou, Y. Shi, X. Chen, S. Li, and J. Li, "Numerical study of an asymmetric equivalent $\lambda/4$ phase shift semiconductor laser for use in laser arrays," *IEEE J. Quantum Electron.*, vol. 47, no. 4, pp. 534–540, Apr. 2011.

[15] Y. Shi, R. Liu, S. Liu, and X. Zhu, "A low-cost and high-wavelength-precision fabrication method for multiwavelength DFB semiconductor laser array," *IEEE Photon. J.*, vol. 6, no. 3, pp. 1–12, May 2014.

[16] Y. Shi *et al.*, "Study of the multiwavelength DFB semiconductor laser array based on the reconstruction-equivalent-chirp technique," *Appl. Opt.*, vol. 31, no. 20, pp. 3243–3250, Oct. 2014.

[17] Available [Online]. https://www.lumerical.com/tcad-products/mode/

[18] Y. Shi *et al.*, "Improved single-mode property of DFB semiconductor laser based on sampling technique using chirp compensation," *IEEE Photon. J.*, vol. 7, no. 1, pp. 1–10, Feb. 2015.

[19] H. Ghafouri-Shiraz, *Distributed Feedback Laser Diodes and Optical Tunable Filters*. New York, NY, USA: Wiley, 2003, pp. 101–106.

[20] L. A. Coldren, S. W. Corzine, and M. L. Masanovic, *Diode Lasers and Photonic Integrated Circuits*, 2nd ed. New York, NY, USA: Wiley, 2012, pp. 149–151.

[21] J.-I. Hashimoto, Y. Nakano, and K. Tada, "Influence of facet reflection on the performance of a DFB laser integrated with an optical amplifier/modulator," *IEEE J. Quantum Electron.*, vol. 28, no. 3, pp. 594–603, Mar. 1992.